# Buckling analysis of functionally graded carbon nanotube-reinforced curved panels under axial compression and shear.

Enrique García-Macías[a,*], Luis Rodriguez-Tembleque[a], Rafael Castro-Triguero[b], Andrés Sáez[a]

[a] *Department of Continuum Mechanics and Structural Analysis, School of Engineering, University of Seville , Camino de los Descubrimientos s/n, E-41092-Seville, Spain*

[b] *Department of Mechanics, University of Cordoba, Campus de Rabanales, Cordoba, CP 14071, Spain*

**Abstract**

The need for high-performance lightweight materials for the design of aerospace structures predicts a remarkable future role of carbon nanotubes (CNTs). In particular, thin curved fuselage panels are widely employed. However, the theoretical difficulties in the underlying differential problem induced by the curvature, as well as a still under development technology of CNT-based composites, the number of studies dealing with buckling behavior of this structural typology is limited. The present study aims to provide some insight into the linear buckling analysis of functionally graded carbon-nanotube reinforced (FG-CNTRC) cylindrical curved panels under compressive and shear loading. Effective properties of materials of the panels reinforced by single-walled carbon nanotubes (SWCNTs) are estimated through a micromechanical model based on either the Eshelby-Mori-Tanaka approach or the extended rule of mixtures. A series of numerical simulations have been carried out to inspect the influence of curvature, panel aspect ratio, the distribution profile of reinforcements (uniform and three non-uniform distributions) and CNTs orientation angle on the buckling critical load under compressive and shear loading in uniform thermal environments. Results demonstrate that the change of fiber orientation, CNTs distribution, panel aspect ratio, loading condition and temperature have noticeable effects on the buckling strength and buckling modes of FG-CNTRC curved panels.

*Keywords:*
Functionally graded Carbon nanotube, Cylindrical panel, Buckling, Shell finite elements, Temperature-dependent properties

## 1. Introduction

The interest in composite materials for the design of aerospace structures has been steadily growing over the last decades. The upsurge in the need for lightweight structures able to give high level performances has led to a more intensive use of advanced materials, such as fiber reinforced composites, laminates, sandwiches, foams and nanostructures [1]. In particular, carbon nanotubes (CNTs) exhibit manifold interesting features as reinforcing fibers for high strength materials [2] and smart materials with self-sensing capabilities [3, 4]. The introduction of composite materials to a larger extent on commercial aircrafts such as Boeing 787 and Airbus A380, predicts a remarkable role of carbon nanotube-reinforced composites (CNTRC) for both aeronautical and aerospace industry [5]. A promising direction is the application of CNTs as reinforcements in Functionally Graded Materials (FGM). This branch of advanced materials is characterized by spatially continuous varying properties [6]. These materials are inhomogeneous composites characterized by smooth and continuous variations in both compositional profile and material properties, feature that eludes characteristic issues of laminates such as delamination and debonding [7–9]. An interesting application of these new materials is on curved fuselage panels. However, due to the mathematical difficulties involved in their formulation, works on prediction of the critical buckling loads of CNTRC cylindrical unstiffened curved panels subjected to uniform axial compression and shear are scarce in the literature.

Papers related to the buckling theory of curved panels are not so numerous in comparison to the literature devoted to flat shell or cylindrical shell buckling. In the case of isotropic curved panels under axial compressive loading, some analytical solutions were proposed under the assumption of critical loads equal to the case of full revolution cylinders. This is the case of the reference expressions developed by Redshaw [10] and Timoshenko [11]. Stowell [12] proposed a modified form of Redshaw's expression taking into account the influence of the

*Corresponding author.
*Email address:* egarcia28@us.es (Enrique García-Macías)

boundary conditions. However, gross differences have been found with these simplifications in comparison to some experimental results in the literature [13–15]. Further investigations were conducted by Yamura et al. [16] who studied numerically the buckling plastic collapse and by Park et al. [17, 18] who provided a simplified method to estimate the ultimate strength based on Faulkner's formule for a single plate with a newly defined slenderness parameter including curvature effect. Le Tran et al. [19] proposed semi-empirical formulae for predicting the elastic buckling and ultimate strength based on finite element simulations. Similar analyses were also conducted for the case of buckling of curved shells under shear loading. The initial analysis were conducted by Legget [20] for long, slightly curved plates under uniform shear stresses. There are some other analytical results in the literature (see e.g. [21, 22]) although due to the nonexistence of simple trigonometric shape functions for shear buckling modes of curved panels, numerical simulations by finite element analysis has proven to be more feasible [23, 24].

With regard to the analysis of CNTRC and FG-CNTRC structural elements, the number of publications has considerably increased in recent years with plenty of newly results. One of the first works concerning non-uniform distributions of CNTs within an isotropic matrix was published by Shen [25]. In this work, a nonlinear vibration analysis of FG-CNTRC plates in thermal environments was presented. Shen and Zhang [26] analyzed the thermal buckling and postbuckling behavior of uniform and symmetric FG-CNTRC plates under in-plane temperature variation. The results showed that functionally graded CNT distributions can rise the buckling temperature as well as the thermal postbuckling strength of plates. However, it is also observed that in some cases the plate with intermediate nanotube concentration may not present intermediate buckling temperature and initial thermal postbuckling strength. Based on the homogenization framework of Eshelby-Mori-Tanaka, Arani et al. [27] investigated analytically and numerically the buckling behavior of moderately thick CNTRC rectangular plates subjected to uniaxial compression. Adopting classical laminate plate theory and third-order shear deformation theory, the authors optimized the orientation of CNTs to achieve the highest critical load. A similar contribution by Mehrabadi et al. [28] analyzed the mechanical buckling of FG-CNT reinforced composite Mindlin plates subjected to both uniaxial and biaxial in-plane loadings. The buckling analysis of FG-CNTRC plates under in-plane mechanical loads was also carried out by Lei et al. [29] using the element-free kp-Ritz method. In that work, a micromechanical model based on either the Eshelby-Mori-Tanaka approach or the extended rule of mixture showed good synergism between both methodologies for the case of uniaxially CNT reinforced composites. Zhu et al. [30] proposed a meshless local Petrov-Galerkin approach based on the moving Kriging interpolation technique for the geometrically nonlinear thermoelastic analysis of FG plates in thermal environments. Later work of the same group dealt with the mechanical and thermal buckling analysis of ceramic-metal FG plates [31]. Lei et al. [32] employed the IMLS-Ritz method for the buckling analysis of thick FG-CNT skew plates resting on Pasternak foundations. Similar results can be found in the literature concerning the buckling analysis of FG-CNTRC thick plates resting on Winkler [33] and Pasternak foundations [34], the buckling analysis of thick FG-CNTRC skew plates under biaxial compression [35], the postbuckling behavior of FG-CNTRC plates with elastically restrained edges under axial compression [36], as well as of biaxial compressed arbitrarily straight-sided quadrilateral ceramic-metal FGM plates [37]. This methodology has been found useful for other manifold applications such as the free vibration of moderately thick laminated CNTRC plates [38] and triangular plates [39], large deformation of FG-CNT reinforced composite quadrilateral plates [40], and FG-CNTRC plates with elastically restrained edges [41]. Those studies concluded that the FG-X profile results in the stiffest CNT configuration, unlike the FG-O profile which generates the least stiff configuration. Similar conclusions were reached by Zhang et al. [42] who investigated the large deflection behavior of FG-CNTRC plates resting on elastic foundations under transversely distributed loads. It is also worth mentioning the proposal of these authors of a state-space Levy method for the vibration analysis of FG-CNTRC plates subjected to in-plane loads based on higher-order shear deformation theory [43]. Nevertheless, the number of publications dealing with cylindrical panels is less numerous. It is noteworthy the work of Lei et al. [44] which presented parametric studies of the dynamic stability of CNTRC-FG cylindrical panels under static and periodic axial forces using the mesh-free-kp-Ritz method and the Eshelby-Mori-Tanaka homogenization scheme. Shen and Xiang [45] employed the higher-order shear deformation theory with a von Kármán-type of kinematic nonlinearity to study the postbuckling of axially compressed FG-CNTRC cylindrical panels resting on elastic foundations in thermal environment.

Regarding the state of the art of mechanical analysis of FG-CNTRC composites [46], only a limited number of works reported on the buckling analysis of FG-CNTRC cylindrical panels under axial compressive and tangential forces. The influence of the different variables involved in the micromechanics of functionally graded materials, such as volume fraction, CNT distributions, fiber orientation angle and temperature-dependent material properties, on the buckling behavior of curved panels is still unexplored. The objective of the present study is to investigate the effect of the main design variables which influence the linear buckling behavior of FG-CNTRC unstiffened curved panels. The panels have been modeled with the commercial FEA software ANSYS v15.0 with effective properties of materials estimated by means of a micromecamechanical model based on either the Eshelby-Mori-

Tanaka approach or the extended rule of mixtures. Detailed parametric studies have been carried out to inspect the influence of curvature, panel aspect ratio, the distribution profile of reinforcements (uniform and three non-uniform distributions) and CNTs orientation angle on the buckling critical load under compressive and shear loading in uniform thermal environments. The results show substantial influence of these variables on the buckling strength and buckling modes of FG-CNTRC curved panels.

The paper is organized as follows. Section 2 introduces the terminology used for the parametrization of FG-CNTRC cylindrical curved panels as well as the homogenization schemes. Section 3 sets up the basis of the eigenvalue buckling analysis of FG-CNTRC cylindrical curved panels. Section 4 presents some comparison analyses with the existing literature, buckling analysis of FG-CNTRC curved panels under axial compressive and tangential forces. Finally, Section 5 presents the conclusions derived from this work.

## 2. FG-CNTRC cylindrical curved panels

The FG-CNTRC cylindrical curved panel and the corresponding local coordinate system $\{u, v, w\}$ considered in this paper are shown in Fig. 1a. This panel is assumed to be thin and of projected width $b$, straight length $a$, radius $R$, span angle $\beta$ and uniform constant thickness $t$. In order to characterize the curvature of the panels, it is defined a non-dimensional parameter $Z = s^2/R \cdot t$ (modified Bartdorf's parameter deprived of the effects of Poisson's ratio), being $s$ the curved length of the panel. From a physical point of view, this parameter is proportional to the sagitta of the curved edges $h$ (given by $b^2/8 \cdot R$) divided by its thickness $t$. In order to visualize the curvature parameter $Z$, the schematic curved shapes of selected curvature parameters are shown in Fig. 1b. The CNTs are assumed to be uniaxially aligned at $\alpha$ degrees with respect to the axial direction (x-axis) and functionally graded along the thickness of the panel by four different distributions, namely UD, FG-V, FG-O and FG-X. UD-CNTRC represents the uniform distribution whilst FG-V, FG-O and FG-X CNTRC are linear distributions of carbon nanotubes along the radial direction. According to these distributions (Fig. 2), the CNT volume fractions $V_{CNT}(z)$ are given by

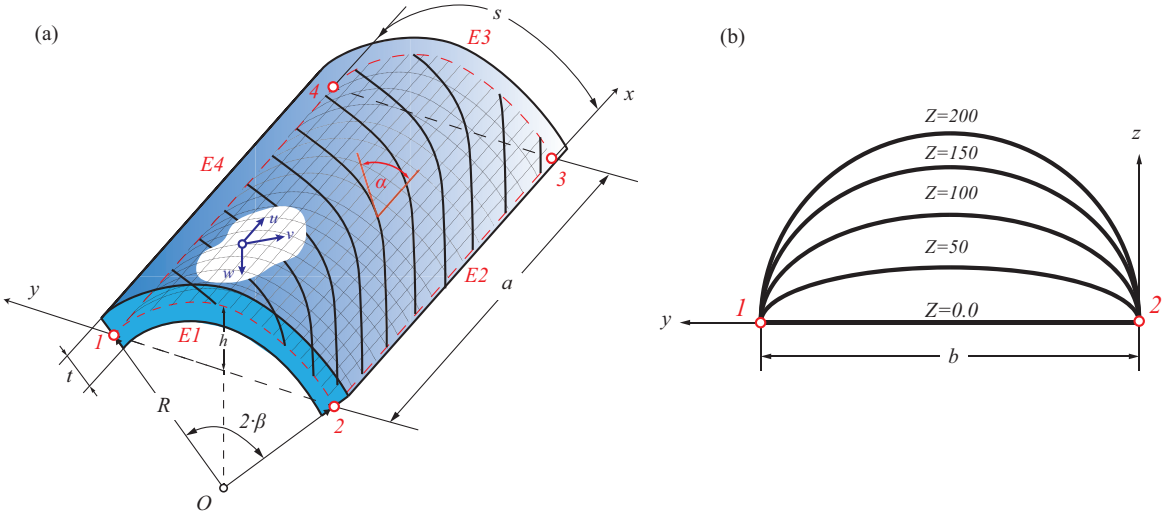


Figure 1: a) Geometry and coordinate system of carbon nanotube nanoreinforced cylindrical panel. b) Schematic views of panels with different curvature parameters $Z$.

$$
\begin{aligned}
V_{CNT} &= V^*_{CNT} && \text{(UD CNTRC)} \\
V_{CNT} &= \tfrac{4|z|}{t} V^*_{CNT} && \text{(FG-X CNTRC)} \\
V_{CNT} &= (1 + \tfrac{2z}{t}) V^*_{CNT} && \text{(FG-V CNTRC)} \\
V_{CNT} &= 2(1 - \tfrac{2|z|}{t}) V^*_{CNT} && \text{(FG-O CNTRC)}
\end{aligned}
\tag{1}
$$

with $V^*_{CNT}$ the volume fraction of CNTs that can be calculated from the mass fraction of nanotubes, $w_{CNT}$, as

$$
V^*_{CNT} = \frac{w_{CNT}}{w_{CNT} + (\rho^{CNT}/\rho^m) - (\rho^{CNT}/\rho^m) w_{CNT}} \tag{2}
$$

where $\rho^m$ and $\rho^{CNT}$ are the densities of the matrix and CNTs, respectively. Hence, the cases of uniformly distributed (UD), i.e. $V_{CNT} = V^*_{CNT}$, and functionally graded (FG) CNTRCs will have the same value of mass fraction of CNTs.

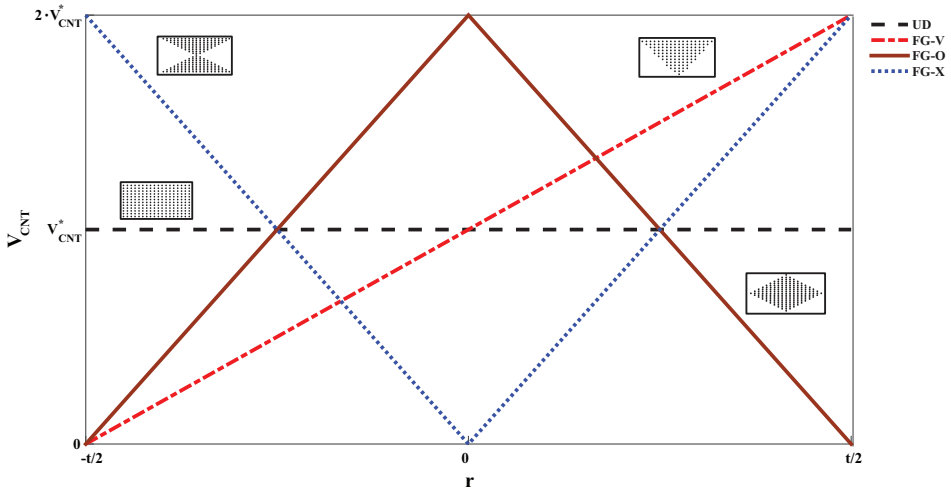


Figure 2: Variation of nanotube volume fraction ($V_{CNT}$) along the radial direction for types of FG-V, FG-O, FG-X and UD.

The effective material properties of the two-phase nanocomposites mixture of uniaxially aligned CNTs reinforcements and a polymeric matrix, can be estimated according to the Mori-Tanaka scheme [47] or the rule of mixtures [48, 49]. The accuracy of the extended rule of mixtures (EROM) has been widely discussed and a remarkable synergism with the Mori-Tanaka scheme for functionally graded ceramic-metal beams is reported in [50].

### *2.1. Extended Rule of Mixtures*

According to the extended rule of mixtures, the effective material properties of CNTRC panels can be expressed as [25]

$$E_{11} = \eta_1 V_{CNT} E_{11}^{CNT} + V_m E^m \tag{3a}$$

$$\frac{\eta_2}{E_{22}} = \frac{V_{CNT}}{E_{22}^{CNT}} + \frac{V_m}{E^m} \tag{3b}$$

$$\frac{\eta_3}{G_{12}} = \frac{V_{CNT}}{G_{12}^{CNT}} + \frac{V_m}{G^m} \tag{3c}$$

where $E_{11}^{CNT}$, $E_{22}^{CNT}$ and $G_{12}^{CNT}$ indicate the Young's moduli and shear modulus of SWCNTs, respectively, and $E^m$ and $G^m$ represent the corresponding properties of the isotropic matrix. In order to account for the scale-dependent material properties, the CNT efficiency parameters, $\eta_j$ ($j$=1,2,3), are introduced and can be calculated by matching the effective properties of the CNTRC obtained from a molecular dynamics (MD) or multi-scale simulation with those from the rule of mixtures. $V_{CNT}$ and $V_m$ are respectively the volume fractions of the carbon nanotubes and matrix, whose sum equals unity. Similarly, the thermal expansion coefficients in the longitudinal and transverse directions, $\alpha_{11}$ and $\alpha_{22}$, Poisson's ratio $\nu_{12}$ and the density $\rho$ of the nanocomposites can be determined in the same way as

$$\nu_{12} = V_{CNT}\nu_{12}^{CNT} + V_m\nu^m \tag{4a}$$

$$\rho = V_{CNT}\rho^{CNT} + V_m\rho^m \tag{4b}$$

$$\alpha_{11} = V_{CNT}\alpha_{11}^{CNT} + V_m\alpha^m \tag{4c}$$

$$\alpha_{22} = (1+\nu_{12}^{CNT})V_{CNT}\alpha_{22}^{CNT} + (1+\nu^m)V_m\alpha^m - \nu_{12}\alpha_{11} \tag{4d}$$

where $\nu_{12}^{CNT}$ and $\nu^m$ are Poisson's ratios, and $\alpha_{11}^{CNT}$, $\alpha_{22}^{CNT}$ and $\alpha^m$ are the thermal expansion coefficients of the CNT and matrix, respectively. Note that $\nu_{12}$ is considered to be constant over the thickness of the functionally graded

CNTRC plates. In addition, we assume that $G_{23} = G_{13} = G_{12}$. The rest of the other effective mechanical properties are defined as follows

$$\begin{aligned} &E_{33} = E_{22}, \quad G_{13} = G_{12}, \quad \nu_{23} = \frac{E_{22}}{2G_{23}} - 1, \\ &\nu_{13} = \nu_{12}, \quad \nu_{31} = \nu_{21}, \quad \nu_{32} = \nu_{23}, \\ &\nu_{21} = \nu_{12}\frac{E_{22}}{E_{11}} \end{aligned} \tag{5}$$

*2.2. Eshelby-Mori Tanaka approach*

The Mori-Tanaka method [51] allows to extension of the theory of Eshelby [52, 53], restricted to one single inclusion in a semi-infinite elastic, homogeneous and isotropic medium, to the case of multiple inhomogeneities embedded into a finite domain. The Eshelby-Mori-Tanaka approach, known as the equivalent inclusion-average stress method, is based on the equivalent elastic inclusion idea of Eshelby and the concept of average stress in the matrix due to Mori-Tanaka. In this paper, we consider a linear elastic polymer matrix reinforced by a large number of dispersed aligned and straight CNTs. According to Benveniste's revision [54], the following expression of the effective elastic tensor is obtained:

$$C = C_m + V_{CNT}\langle (C_r - C_m)\, A_r \rangle \left(V_m I + V_{CNT}\langle A_r \rangle\right)^{-1} \tag{6}$$

where $I$ is the identity tensor, $C_m$ is the stiffness tensor of the equivalent fiber, $C_r$ is the stiffness tensor of the equivalent fiber, and $A_r$ is the dilute mechanical strain concentration tensor for the fiber:

$$A_r = \left[I + S\,(C_m)^{-1}\,(C_r - C_m)\right]^{-1} \tag{7}$$

The tensor $S$ is the Eshelby's tensor, as given by Eshelby [52] and Mura [55]. The terms enclosed with angle brackets in Eq. 6 represent the average value of the term over all orientations defined by transformation from the local fiber coordinates $(o - x_1' x_2' x_3')$ to the global coordinates $(o - x_1 x_2 x_3)$(Fig. 3). The matrix is assumed to be elastic and isotropic, with Young's modulus $E_m$ and Poisson's ratio $\nu_m$. Each straight CNT is modeled as a long fiber with transversely isotropic elastic properties. Therefore, the composite is also transversely isotropic. The substitution of the non-vanishing components of the Eshelby's tensor $S$ for a straight, long fiber along the $x_2$-direction in Eq. 7 gives the dilute mechanical strain concentration tensor. Then the substitution of $A_r$ (Eq. 7) into Eq. 6 gives the tensor of effective elastic moduli of the composite reinforced by aligned and straight CNTs. In particular, the Hill's elastic moduli are found as [47]:

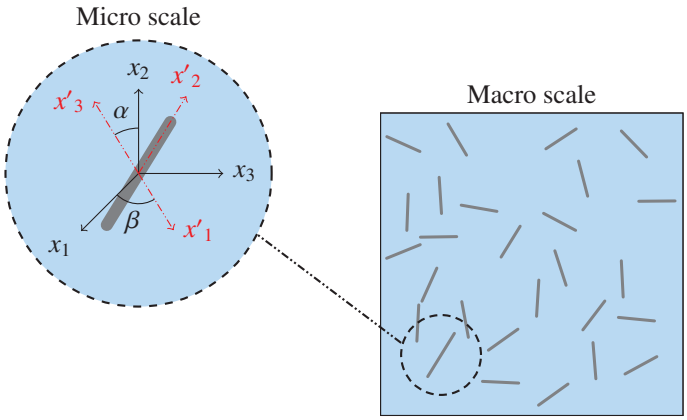


Figure 3: Representative volume element (RVE) including straight CNTs.

$$k = \frac{E_m\{E_m V_m + 2k_r(1+\nu_m)[1 + V_{CNT}(1-2\nu_m)]\}}{2(1+\nu_m)[E_m(1+V_{CNT}-2\nu_m) + 2V_m k_r(1-\nu_m-2\nu_m^2)]} \tag{8}$$

$$l = \frac{E_m\{\nu_m V_m[E_m + 2k_r(1+\nu_m)] + 2V_{CNT}k_r(1-\nu_m^2)\}}{(1+\nu_m)[E_m(1+V_{CNT}-2\nu_m) + 2V_m k_r(1-\nu_m-2\nu_m^2)]} \tag{9}$$

$$\begin{aligned} n = &\frac{E_m^2 V_m(1+V_{CNT}-V_m\nu_m) + 2V_m V_{CNT}(k_r n_r - l_r^2)(1+\nu_m)^2(1-2\nu_m)}{(1+\nu_m)[E_m(1+V_{CNT}-2\nu_m) + 2V_m k_r(1-\nu_m-2\nu_m^2)]} \\ &+ \frac{E_m[2V_m^2 k_r(1-\nu_m) + V_{CNT}n_r(1+V_{CNT}-2\nu_m) - 4V_m l_r \nu_m]}{E_m(1+V_{CNT}-2\nu_m) + 2V_m k_r(1-\nu_m-2\nu_m^2)} \end{aligned} \tag{10}$$

$$p = \frac{E_m[E_m V_m + 2p_r(1+\nu_m)(1+V_{CNT})]}{2(1+\nu_m)[E_m(1+V_{CNT}) + 2V_m p_r(1+\nu_m)]} \tag{11}$$

$$k = \frac{E_m[E_m V_m + 2m_r(1+\nu_m)(3+V_{CNT}-4\nu_m)]}{2(1+\nu_m)\{E_m[V_m + 4V_{CNT}(1-\nu_m)] + 2V_m m_r(3-\nu_m-4\nu_m^2)\}} \tag{12}$$

where $k$, $l$, $m$, $n$ and $p$ are Hill's elastic moduli of the composite; $k$ is the plane-strain bulk modulus normal to the fiber direction, $n$ is the uniaxial tension modulus in the fiber direction, $l$ is the associated cross modulus, $m$ and $p$ is the shear moduli in planes normal and parallel to the fiber direction, respectively. $k_r$, $l_r$, $m_r$, $n_r$ and $p_r$ are the Hill's elastic moduli for the reinforcing phase (CNTs). The material properties of the composite can be expressed in terms of engineering constants as [56]:

$$E_{11} = n - \frac{l^2}{k} \tag{13}$$

$$E_{22} = \frac{4m(k-l^2)}{kn - l^2 + mn} \tag{14}$$

$$\nu_{12} = \nu_{13} = \frac{l}{2k} \tag{15}$$

$$\nu_{23} = \frac{n(k-m) - l^2}{n(k+m) - l^2} \tag{16}$$

$$G_{12} = G_{13} = p \tag{17}$$

## 3. Formulation of eigenvalue buckling analysis of FG-CNTRC cylindrical curved panels

The numerical studies of eigenvalue buckling analysis are conducted with the coomercial software ANSYS v15.0. The panel is modeled with the standard structural shell element, Shell 181 [57]. This element type is a quadrilateral 4-nodes element involving both bending and membrane properties with three rotational and three translational degrees of freedom per node. This element is suitable for thin to moderately-thick shell structures. The aim of this paper is focused on the study of the linear buckling of simply supported cylindrical curved panels subjected to axial pressure and shear forces. Hence, the boundary conditions considered in the modeling procedure are summarized in Table 1. Note that the boundary conditions are defined correspondingly in the local cylindrical coordinates $\{u, v, w\}$ as represented in Fig. 1a.

Table 1: Boundary conditions for buckling under axial compression and tangential forces

| | Compression | | | Shear | | |
|---|---|---|---|---|---|---|
| | u | v | w | u | v | w |
| Corner 1 | cpl | 0 | 1 | 1 | 1 | 1 |
| Corner 2 | cpl | 0 | 1 | 1 | 0 | 1 |
| Corner 3 | 1 | 0 | 1 | 1 | 0 | 1 |
| Corner 4 | 1 | 1 | 1 | 1 | 0 | 1 |
| Edge 1 | cpl | 0 | 1 | 0 | 0 | 1 |
| Edge 2 | 0 | 0 | 1 | 0 | 0 | 1 |
| Edge 3 | 1 | 0 | 1 | 0 | 0 | 1 |
| Edge 4 | 0 | 0 | 1 | 0 | 0 | 1 |

(cpl coupled; 1 restrained; 0 free).

The theoretical background of this procedure consists on the application of an arbitrary reference level of external load $\{R\}_{ref}$, and perform a standard linear analysis to determine element stresses. The effects of membrane stresses on the lateral deflection are accounted for by the stress stiffness matrix $[K_\sigma]_{ref}$ which augments the conventional stiffness matrix $[K]$. For a generic load level, obtained by multiplying the reference load by the scalar $\lambda$, the stress stiffness matrix can be written

$$[K_\sigma] = \lambda\,[K_\sigma]_{ref}\,; \quad \{R\} = \lambda\,\{R\}_{ref} \tag{18}$$

Eqs. 18 imply that multiplication of all loads $R_i$ in $\{R\}$ by $\lambda$ also multiplies the intensity of the stress field by $\lambda$ but does not alter the distribution of stresses. Because the problem is assumed linear, the conventional stiffness

matrix $[K]$ does not depend on loading. Let buckling displacements $\{\delta D\}$ take place relative to displacements $\{D\}_{ref}$ of the reference configuration. Then because the external loads do not change at a bifurcation point, we have

$$\begin{cases} ([K] + \lambda_{cr}[K_\sigma])\{D\}_{ref} = \lambda_{cr}\{R\}_{ref} \\ ([K] + \lambda_{cr}[K_\sigma])\Big(\{D\}_{ref} + \{\delta D\}\Big) = \lambda_{cr}\{R\}_{ref} \end{cases} \tag{19}$$

Subtraction of the first equation from the second yields

$$([K] + \lambda_{cr}[K_\sigma])\{\delta D\} = 0 \tag{20}$$

Eq. 20 is an eigenvalue problem whose smallest root $\lambda_{cr}$ defines the smallest level of external load for which the bifurcation takes place, namely

$$\{R\}_{cr} = \lambda_{cr}\{R\}_{ref} \tag{21}$$

The eigenvector $\{\delta D\}$ associated with $\lambda_{cr}$ is the buckling mode. Eq. 20 can be rewritten in a more compact way as $[K]_{net}\{\delta D\} = 0$. Because forces of this new problem are zero, it can be said that the stresses of critical intensity lead the net stiffness to be singular with respect to the buckling mode $\{\delta D\}$. Mathematically, $[K]_{net}$ has a zero determinant thus the linear bifurcation problem reduces to the following eigenvalue problem

$$\Big|[K] + \lambda_{cr}[K_\sigma]_{ref}\Big| = 0 \tag{22}$$

Finally, in order to implement the constitutive equations of the resulting CNTRCs into the modeling, the preintegrated sections module of ANSYS is employed. This module permits the specification of the membrane, bending and coupling stiffness matrices of the shells. For this purpose, let the constitutive equations of the CNTRCs written in Voigt's notation as follows

$$\begin{bmatrix} s_{11} \\ s_{22} \\ s_{12} \\ s_{23} \\ s_{13} \end{bmatrix} = \begin{bmatrix} Q_{11}(z) & Q_{12}(z) & 0 & 0 & 0 \\ Q_{12}(z) & Q_{22}(z) & 0 & 0 & 0 \\ 0 & 0 & Q_{66}(z) & 0 & 0 \\ 0 & 0 & 0 & Q_{44}(z) & 0 \\ 0 & 0 & 0 & 0 & Q_{55}(z) \end{bmatrix} \cdot \begin{bmatrix} \gamma_{11} \\ \gamma_{22} \\ \gamma_{12} \\ \gamma_{23} \\ \gamma_{13} \end{bmatrix} \tag{23}$$

$$\begin{array}{lll} Q_{11} = \frac{E_{11}}{1-\nu_{12}\nu_{21}}, & Q_{22} = \frac{E_{22}}{1-\nu_{12}\nu_{21}}, & Q_{12} = \frac{\nu_{21}E_{11}}{1-\nu_{12}\nu_{21}}, \\ Q_{66} = G_{12}, & Q_{44} = G_{23}, & Q_{55} = G_{13} \end{array} \tag{24}$$

where $E_{11}$ and $E_{22}$ are effective Young's moduli of CNTRC panels in the local coordinates; $G_{12}$, $G_{13}$ and $G_{23}$ are the shear moduli; $\nu_{12}$ and $\nu_{12}$ are Poisson's ratios obtained by the extended rule of mixtures (EROM) or the Eshelby-Mori-Tanaka approach. Note that $Q_{ij}$ varies with $z$ according to the grading profile of the CNTRC along the thickness. Thus, the components of the extensional stiffness $C_E$, bending extensional coupling stiffness $C_C$, bending stiffness $C_B$, and transverse shear stiffness $C_S$ are defined by the following integrals

$$\begin{array}{l} (C_E^{ij}, C_C^{ij}, C_B^{ij}) = \int_{-t/2}^{t/2} Q_{ij}(z)\cdot(1, z, z^2)dz \quad (i, j = 1, 2, 6), \\ C_S^{ij} = \frac{1}{ks}\int_{-t/2}^{t/2} Q_{ij}(z)dz \quad (i, j = 4, 5) \end{array} \tag{25}$$

where $ks$ denotes the transverse shear correction factor for FGM, given by [58]

$$ks = \frac{6 - (\nu_{12}^{CNT}V_{CNT} + \nu^m V_m)}{5} \tag{26}$$

## 4. Results and discussion

In this section, several numerical examples are presented to study the buckling behavior of FG-CNTRC curved panels under uniform axial compression and shear in uniform thermal environment. Poly{(*m*-phenylenevinylene) -*co*-[(2,5-dioctoxy-*p*-phenylene)vinylene]} (PmPV) is considered as the matrix and the mean material properties are assumed to be $\nu^m = 0.34$, $\rho^m = 1.15g/m^3$ and $E^m$=(3.52 − 0.0047$T$)GPa, where $T = T_0 + \Delta T$ and room temperature $T_0 = 300$K. The armchair (10,10) SWCNTs are selected as reinforcements. For the Eshelby-Mori-Tanaka approach, we use the the analytical results of Popov et al. [59]. In the case of the extended rule of mixtures, the properties of SWCNTs are taken from the MD simulation carried out by Shen and Zhang [26] and summarized in Table 2. The key issue for the successful application of the extended rule of mixtures to CNTRCs

relies on the CNT efficiency parameters $\eta_j (j=1,2,3)$. In the present study, the CNT efficiency parameters are determined by matching the Young's moduli $E_{11}$ and $E_{22}$ from the MD simulations given by Han and Elliot [60] with the counterparts computed by the rule of mixtures. For example, $\eta_1 = 0.149$ and $\eta_2 = 0.934$ for the case of $V^*_{CNT} = 0.11$, and $\eta_1 = 0.150$ and $\eta_2 = 0.941$ for the case of $V^*_{CNT} = 0.14$, and $\eta_1 = 0.149$ and $\eta_2 = 1.381$ for the case of $V^*_{CNT} = 0.17$. In addition, we assume that $\eta_3 = \eta_2$. Unless otherwise specified, the Eshelby-Mori-Tanaka approach is applied to predict effective material properties of CNTRCs. For the subsequent analyses, it is set up a constant length of b=100cm and thickness t=b/50. In order to define the mesh density, convergence studies of panels with two different aspect ratios, namely a/b=1 and a/b=2, have first been performed as represented in Fig. 4. Different uniform mesh divisions of (a/b)8×8, (a/b)16×16, (a/b)32×32, (a/b)64×64 and (a/b)128×128 have been used, wherein (a/b)64×64 was found to provide accurate results and has been used for all the following results.

Table 2: Temperature-dependent material properties for (10,10) SWCNT ($L$=9.26 nm, $R$=0.68 nm, $h$=0.067 nm, $\nu_{12}^{CNT} = 0.175$)

| Temperature (K) | $E_{11}^{CNT}$ (TPa) | $E_{22}^{CNT}$ (TPa) | $G_{12}^{CNT}$ (TPa) | $\alpha_{11}^{CNT}$ ($\times 10^{-6}$/K) | $\alpha_{22}^{CNT}$ ($\times 10^{-6}$/K) |
|---|---|---|---|---|---|
| 300 | 5.6466 | 7.0800 | 1.9445 | 3.4584 | 5.1682 |
| 400 | 5.5679 | 6.9814 | 1.9703 | 4.1496 | 5.0905 |
| 500 | 5.5308 | 6.9348 | 1.9643 | 4.5361 | 5.0189 |
| 700 | 5.4744 | 6.8641 | 1.9644 | 4.6677 | 4.8943 |
| 1000 | 5.2814 | 6.6220 | 1.9451 | 4.2800 | 4.7532 |

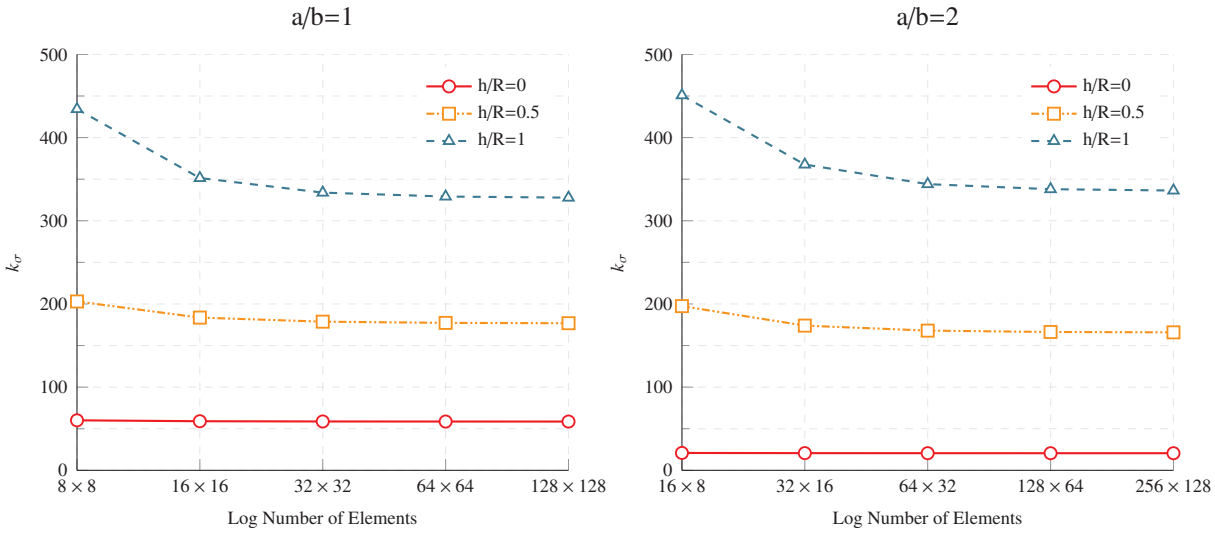


Figure 4: Convergence analysis of the buckling load intensity factor $k_\sigma = \frac{\sigma_{cr}}{\sigma_E}$ of UD-CNTRC panels subjected to axial compression (SSSS, b=100cm, t=b/50, R=b/2, $V^*_{CNT}$=0.11) for different panel aspect ratios: a) a/b=1 and b) a/b=2.

### *4.1. Comparison studies*

First, we carry out several numerical experiments to validate the present computational approach. However, since no results are available in the literature for FG-CNTRC curved panels, the comparison studies focus on the cases of simply supported (SSSS) orthotropic flat shells and isotropic curved panels, configurations which do have analytical solutions and are provided in the literature. In addition, the results obtained from the present computational approach are also compared to results available in the literature on the buckling behavior of FG-CNTRC flat panels.

#### *4.1.1. Orthotropic flat shells*

The case of orthotropic rectangular shells (Z=0, a×b) subjected to compressive edge forces was studied by Hwang and Lee [61]. In the case of buckling under uniaxial compression of simply supported shells, closed solutions are provided as follows:

$$\frac{\sigma_{cr}}{\sigma_o} = \frac{m^2}{R^2} + \frac{\chi^2}{m^2} + 2\eta \tag{27}$$

where $\sigma_{cr}$ is the critical buckling stress and $m$ is the number of half-waves in the loading direction. The terms $\sigma_o$, $R$, $\lambda$ and $\eta$ are defined as:

$$\sigma_o = \frac{\pi^2 \sqrt{D_{11} D_{22}}}{b^2 h}; \quad \chi = \lambda^{1/4}(a/b) \tag{28}$$

$$\lambda = \frac{D_{22}}{D_{11}}; \quad \eta = \frac{D_{12} + 2D_{66}}{\sqrt{D_{11} D_{22}}} \tag{29}$$

with $D_{ij}$ the flexural rigidities of the shell. The width $b$ and thickness $t$ of the shell are set to 1m and t=0.021m, respectively, and the Young's modulus in x-direction $E_x$=1.81 $\times$ $10^{11} N/m^2$, Young's modulus in y-direction $E_y$=1.03 $\times$ $10^{10} N/m^2$, shear modulus $G_{xy}$=7.53 $\times$ $10^9 N/m^2$ and Poisson's ratio $\nu_{xy}$ = 0.28. Buckling load parameters for the first $m$ parameters ($m = 1, \ldots, 5$) are depicted in Fig. 5. Here, it is observed that the number of buckle waves increases as the plate aspect ratio increases. Note that each mode shape takes place in a range of aspect ratios, and the buckling mode changes when there is a change in the energy state of the plate. In the case of the present computational approach, the first critical buckling load is represented which corresponds to the buckling mode with the lowest energy state, associated with the buckling eigenvalue problem, and thus it provides the minimum envelope of the analytical curves.

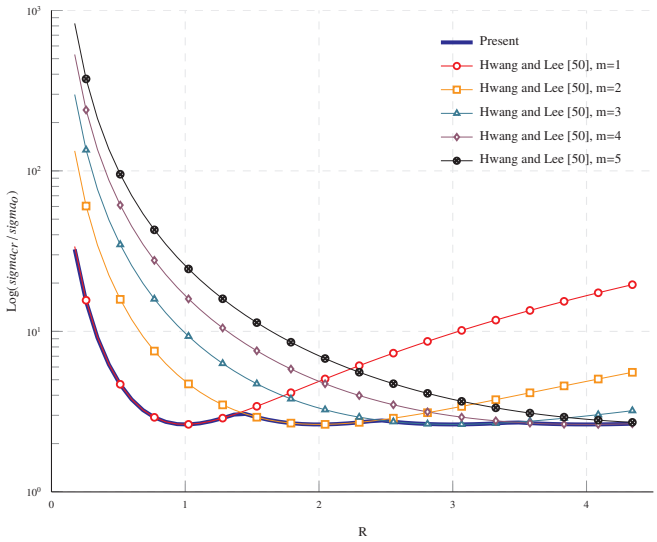


Figure 5: Comparison analysis of the critical buckling stress $\sigma_{cr}/\sigma_o$ as a function of the adjusted plate aspect ratio $R$ for the first five buckling modes ($m = 1, \ldots, 5$) of a simply supported rectangular orthotropic plate.

*4.1.2. Isotropic curved panels*

In this second test, the results of the present approach for unstiffened curved isotropic panels are compared to the theoretical formulae found in the literature. In particular, the numerical values of the critical buckling load are compared to the reference analytical expressions proposed by Redshaw [10], Timoshenko [11], Stowell [12] and Domb and Leigh [62], whose expressions are collected in [19]. In order to simplify the comparison, all the results are expressed by the so-called load intensity factor $k_\sigma$ defined by

$$k_\sigma = \frac{\sigma_{cr}}{\sigma_E}; \quad \sigma_E = \frac{\pi^2 E}{12(1-\nu^2)} \left(\frac{t}{s}\right)^2 \tag{30}$$

The results of this comparison are presented in Fig. 6 where the load intensity factor $k_\sigma$ is plotted as a function of the curvature parameter $Z$. For values of $Z$ tending towards zero, all formulae naturally converge to $k_\sigma = 4$ corresponding to the case of flat square plate. It is also remarkable that, for all curves, the buckling coefficients increase with $Z$. This tendency is due to the fact that for increasing values of $Z$, larger curvature values lead to higher circumferential membrane stresses in the radial direction. Nonetheless, some differences can be found in the asymptotic behavior of these methodologies. In the case of the formulae of Redshaw and Timoshenko, the buckling coefficients asymptotically converge towards a straight line with slope equal to the buckling coefficient of a revolution cylinder. On the contrary, the formulae of Domb and Leigh, Stowell and the present numerical approach converge towards half this value. These differences can be attributed to the different boundary conditions considered in these two sets of approaches. The assumption of a full revolution cylinder of the first set of formulae

assumes four free cut edges, whereas the refined boundary conditions for curved panels of the second set of approaches only consider two.

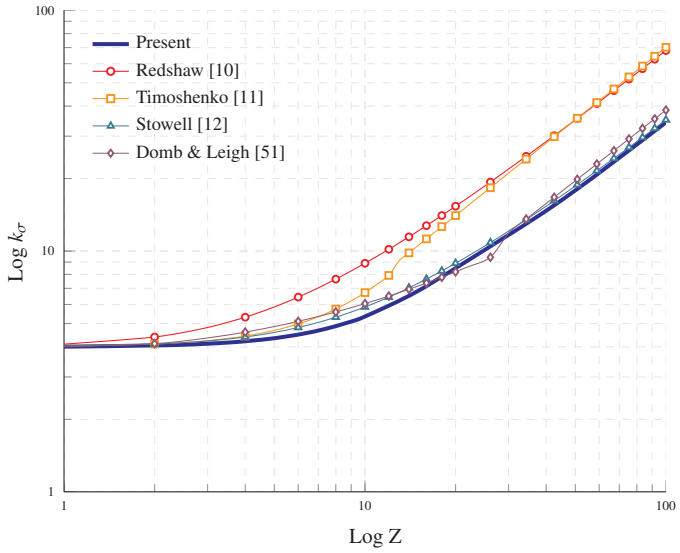


Figure 6: Comparison of the reference analytical buckling coefficients with the present numerical results.

### *4.1.3. FG-CNTRC flat panels*

Finally, the present computational approach has been also compared to the results provided by Lei et al. [29] with the element-free kp-Ritz method for the buckling behavior of FG-CNTRC flat panels subjected to uniaxial compression. Table 3 shows the comparison of the buckling load parameter $\overline{N}_{cr} = N_{cr}b^2/(E_m t^3)$ of various types of CNTRC plates with different boundary conditions, namely simply supported (SSSS), fully clamped (CCCC) and simply supported with one free edge (SSSF). Width-to-thickness ratio of the plates is set to be $b/t$=10 and CNT volume fraction is taken to be $V^*_{CNT}$=0.11. The effective material properties of CNTRCs plates have been estimated by both the extended rule of mixture and the Eshelby-Mori-Tanaka approach. It can be seen that the results obtained by the proposed methodology math very well with the cited reference. Furthermore, the buckling load parameter obtained by the extended rule of mixture agrees well with the solution of Eshelby-Mori-Tanaka approach. Consistent with many previously published works, this result supports the convenience of the use of the simple extended rule of mixtures in the case of uniaxially CNT reinforced composite. Nonetheless, the micromechanics model of Eshelby-Mori-Tanaka allows to model a greater number of effects such as agglomeration of nanoinclusions, random distribution of fillers or waviness [47, 50, 56, 63, 64].

Table 3: Comparison study of the buckling load parameter $\overline{N}_{cr} = N_{cr}b^2/\left(E_m t^3\right)$ for UD, FG-O and FG-X CNTRC flat panels under uniaxial compression and different boundary conditions ($a$=$b$, $b/t$=10, $V^*_{CNT}$=0.11).

| Mode | Boundary conditions | | | | | | | | |
|---|---|---|---|---|---|---|---|---|---|
| | SSSS | | | CCCC | | | SSSF | | |
| | Ref. [29] | EMT | EROM | Ref. [29] | EMT | EROM | Ref. [29] | EMT | EROM |
| UD | | | | | | | | | |
| 1 | 14.11 | 14.33 | 14.19 | 25.73 | 25.10 | 24.94 | 12.31 | 12.79 | 12.77 |
| 2 | 23.31 | 24.50 | 24.40 | 26.28 | 27.13 | 27.00 | 16.68 | 17.07 | 16.75 |
| 3 | 25.65 | 28.44 | 27.15 | 29.67 | 31.12 | 30.98 | 22.54 | 23.91 | 23.84 |
| FG-O | | | | | | | | | |
| 1 | 9.83 | 9.97 | 9.85 | 21.12 | 20.30 | 20.15 | 7.90 | 8.24 | 8.23 |
| 2 | 18.61 | 19.64 | 19.55 | 22.85 | 23.74 | 23.64 | 12.60 | 12.79 | 12.51 |
| 3 | 23.04 | 24.45 | 23.30 | 27.41 | 28.12 | 27.69 | 17.71 | 18.87 | 18.83 |
| FG-X | | | | | | | | | |
| 1 | 17.06 | 17.38 | 17.24 | 27.89 | 27.52 | 27.35 | 15.35 | 15.97 | 15.94 |
| 2 | 25.62 | 26.93 | 26.82 | 27.93 | 28.74 | 28.62 | 19.52 | 20.09 | 19.76 |
| 3 | 26.67 | 30.41 | 30.04 | 30.45 | 32.06 | 31.92 | 24.90 | 26.41 | 26.33 |

### 4.2. Results for FG-CNTRC curved panels

The results obtained by the proposed methodology have been shown to be stable and similar to those provided in the literature. Some new results are now presented for unstiffened curved FG-CNTRC panels subjected to axial compression and tangential forces. All the foregoing results are defined by the non-dimensional buckling load intensity factor as follows

$$k_\sigma = \frac{\sigma_{cr}}{\sigma_E}; \quad \sigma_E = \frac{\pi^2 E_m}{12(1-\nu_m^2)}\left(\frac{t}{s}\right)^2 \tag{31}$$

#### 4.2.1. FG-CNTRC Curved panels under axial compression

The cylindrical shells are considered simply supported on all edges (w=0); along the curved edge 1 (loaded one) the longitudinal displacements are allowed but restricted while in the curved edge 3 are restrained (see Fig. 1). The straight edges 2 and 3 are free to wave in the circumferential direction as stated in Table 1. The external load is introduced by means of an external uniform compression on the edge 1 in the longitudinal direction.

The effect of the fiber orientation angle $\alpha$ on the critical buckling load is analyzed for different reinforcement distributions and curvature in Fig. 7. The results show that in the case of flat shells ($h/R$=0) the buckling load intensity factor presents positive curvature with respect to the fiber angle $\alpha$. This fact favors the origin of peak values for fibers approximately aligned with the diagonal direction of the shell. Moreover, among the different distributions of CNTs, FG-X distribution leads to the largest buckling loads whilst the FG-O distribution conducts to the minimum values. This is because the profile of the reinforcement distribution affects the stiffness of the shells. This circumstance points out the advantage of FG materials, in which a desired stiffness can be achieved by adjusting the distribution of CNTs along the thickness direction of the shells. It is concluded that reinforcements distributed close to the top and bottom induce higher stiffness values of shells [65]. Another essential aspect is the influence of the fiber direction. In the case of flat shells, for every reinforcement distribution the critical buckling load increases up to 40% with respect to the shells with fibers aligned with the axial direction. In the case of curved shells ($h/R$=0.9), the curvature significantly increases the buckling load values with respect to the flat configuration. However, this more complex geometry distorts the relationship between the buckling load factor and the fiber orientation angle. It is noticeable that despite the fiber distributions conserve their relative order, there is a range of angles, approximately between 70° and 85°, in which they do not show a significant difference. The effect of the curvature is clarified in Fig. 8 with the analysis of the relationship between the buckling load factor and fiber angle for CNT uniform distribution and different ratios $h/R$. In this figure, it is highlighted the stiffening effect of the curvature. Furthermore, the curves change from a positive curvature with one clear maximum peak to curves with two maximum and one minimum peaks. Similar conclusions can be extracted by varying the CNTs volume fraction $V^*_{CNT}$ as in Fig. 9. In this figure, it is represented the buckling load intensity factor for different fiber orientation angles $\alpha$ and UD-CNTRC panels with increasing CNT volume fractions. The results show that the buckling load intensity factors have higher values when the volume fraction of CNT is larger as it raises the stiffness of the panels. The curvature parameter $Z$ and the fiber angle $\alpha$ also have a substantial influence on the shape of the first buckling mode as can be clearly seen in Figs. 10 and 11.

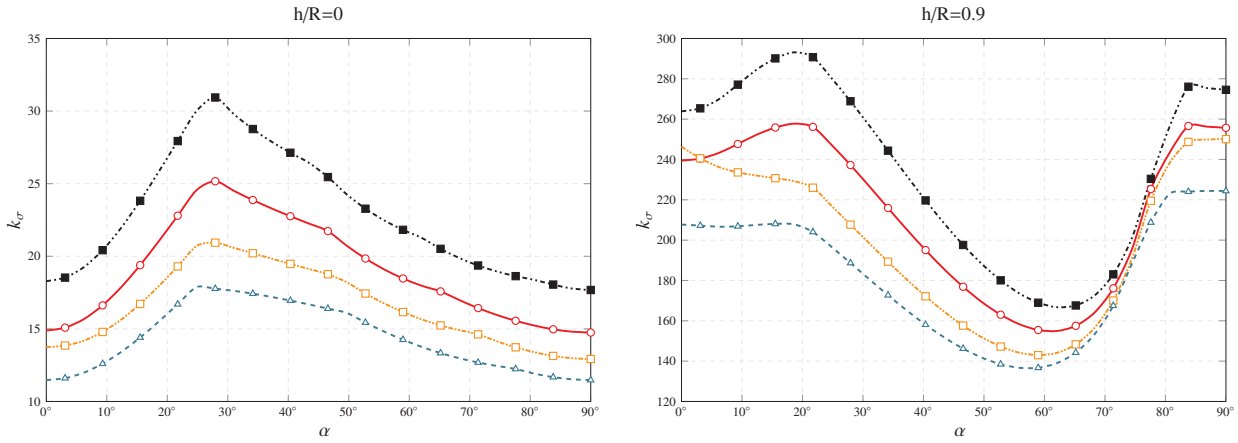


Figure 7: Effect of fiber angle $\alpha$ on the buckling load intensity factor $k_\sigma$ of a FG-CNTRC panel subjected to compressive forces $\alpha$ (SSSS, b=100cm, a=2· b, t=b/50, R=b/2, $V^*_{CNT}$=0.11) for different profiles: UD (—○—), FG-V (··□··), FG-O (- -△- -) and FG-X (- -■- -·)

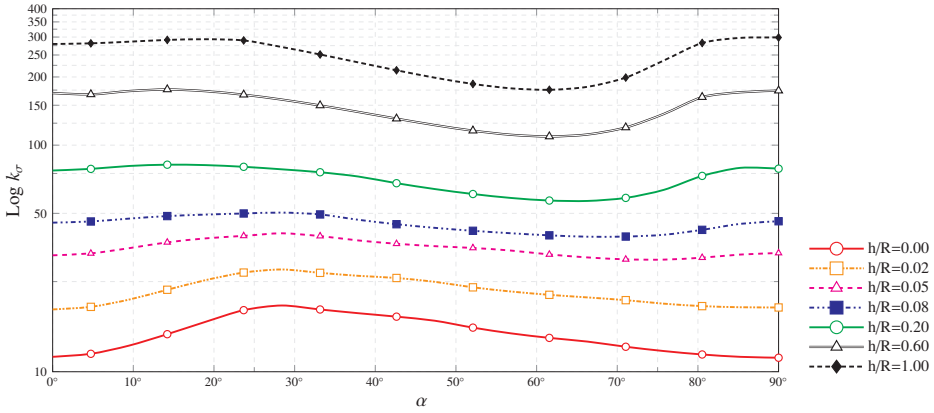


Figure 8: Effect of fiber angle $\alpha$ on the buckling load intensity factor $k_\sigma$ of a UD-CNTRC panel subjected to compressive forces $\alpha$ (SSSS, b=100cm, a=2· b, t=b/50, $V^*_{CNT}$=0.11) for different $h/R$ ratios

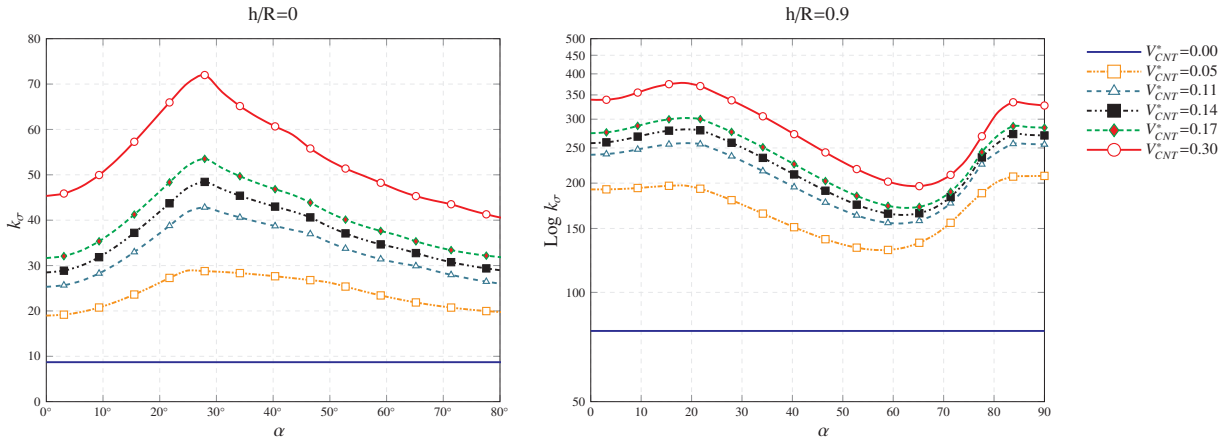


Figure 9: Effect of fiber angle $\alpha$ on the buckling load intensity factor $k_\sigma$ of a UD-CNTRC panel subjected to compressive forces $\alpha$ (SSSS, b=100cm, a=2· b, t=b/50, R=b/2) for different SWCNT volume fractions

Fig. 12 shows the buckling load parameters for simply supported FG-CNTRC curved panels with aspect ratio a/b changing from 0.5 to 8. It can be seen that the buckling load parameters decrease as the plate aspect ratio increases due to the activation of buckling modes with higher number of waves. I is also noticeable that the FG-V and UD distributions show similar results in the curved configuration. This fact, which can also be observed in Fig. 7, results in the inversion of the order of these two curves for certain values of fiber orientation angles and aspect ratios.

Effects of different uniform temperature environments (T=300, 400 and 500K) on the buckling load parameters of FG-CNTRC curved panels with different reinforcement distributions are shown in Table 4. For this study, the extended rule of mixtures is used to predict the effective material properties of CNTRCs. It can be seen that the buckling load intensity factors decrease as temperature increases. This is because an increment of the temperature reduces the elastic moduli of CNTRCs shells since material properties of the matrix and SWCNTs are assumed to be temperature-dependent. As in previous analyses, we also found here that FG-X and FG-O CNTRC shells have the highest and lowest values of buckling load intensity factors, respectively, in different temperature environments.

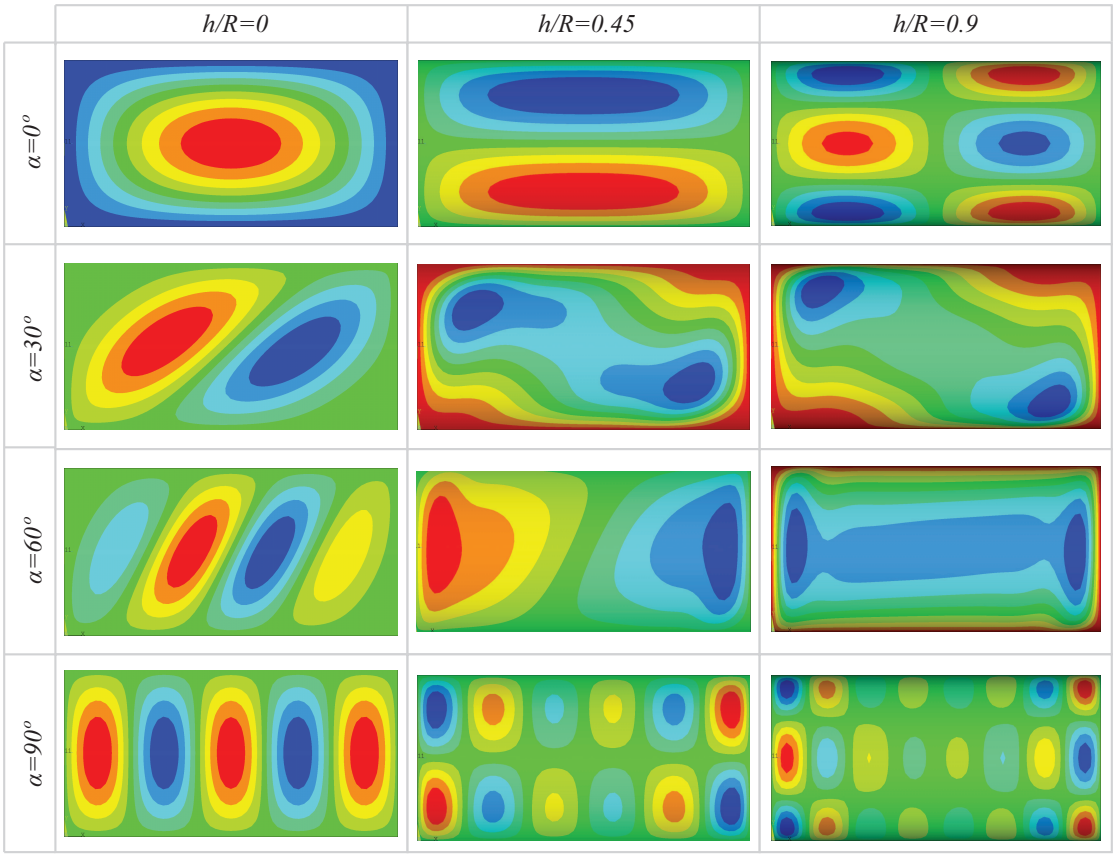


Figure 10: First elastic buckling modes for UD-CNTRC flat panel ($h/R = 0$) and curved panels ($h/R = 0.45, 0.9$) subjected to compressive loading for different fiber orientation angles ($\alpha$) (SSSS, b=100cm, a=2· b, t=b/50, $V^*_{CNT}$=0.11).

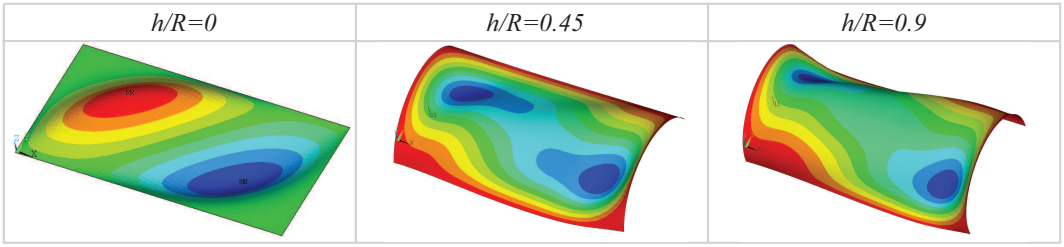


Figure 11: First elastic buckling modes for UD-CNTRC flat panel ($h/R = 0$) and curved panels ($h/R = 0.45, 0.9$) subjected to compressive loading with fiber orientation angle ($\alpha$) of 30° (SSSS, b=100cm, a=2· b, t=b/50, $V^*_{CNT}$=0.11).

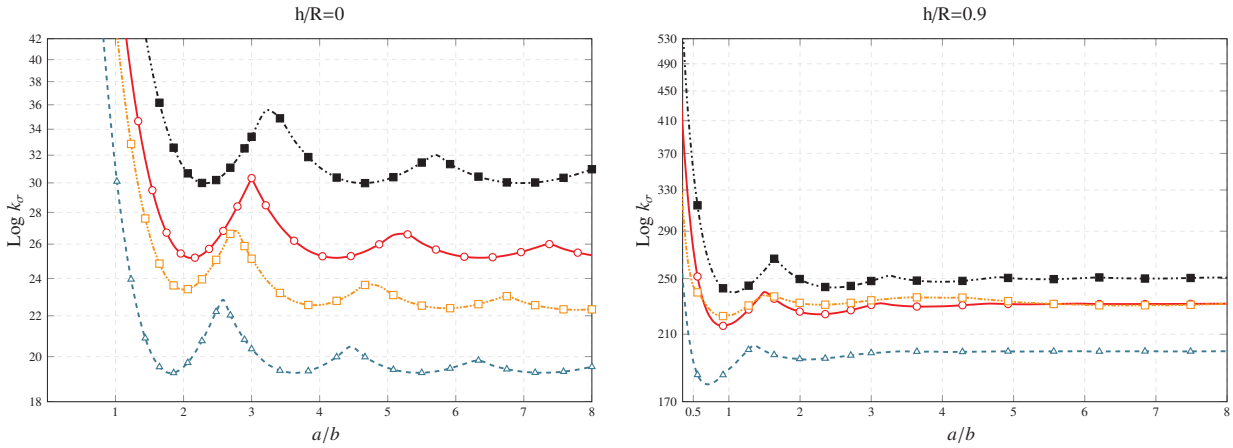


Figure 12: Variation of the buckling load intensity factor $k_\sigma$ of FG-CNTRC panels versus plate aspect ratio under axial compression (SSSS, b=100cm, t=b/50, $V^*_{CNT}$=0.11, $\alpha$=0°) for different profiles: UD (—○—), FG-V (-·-□-·-), FG-O (- -△- -) and FG-X (- -■- -·-).

Table 4: Effect of environment temperature on the buckling load intensity factor ($k_\sigma$=$\sigma_{cr}/\sigma_E$; $\sigma_E$=$\left(\pi^2 E_{(m,T=300K)}/12\left(1-\nu^2_{(m,T=300K)}\right)\right)(t/s)^2$) of FG-CNTRC curved panels under axial compression (SSSS, b=100cm, a=2· b, t=b/50, $V^*_{CNT}$=0.11, $\alpha$=0°).

| T (K) | h/R | Type of CNTRC | | | |
|---|---|---|---|---|---|
| | | UD | FG-V | FG-O | FG-X |
| 300 | 0 | 15.57 | 13.76 | 10.52 | 20.68 |
| | 0.45 | 121.13 | 120.76 | 99.79 | 131.73 |
| | 0.9 | 268.10 | 268.04 | 223.02 | 310.36 |
| 400 | 0 | 12.66 | 10.80 | 7.86 | 17.45 |
| | 0.45 | 74.04 | 77.06 | 65.65 | 81.95 |
| | 0.9 | 176.42 | 176.33 | 145.27 | 192.27 |
| 500 | 0 | 9.41 | 7.56 | 5.15 | 13.41 |
| | 0.45 | 23.27 | 23.93 | 17.76 | 28.56 |
| | 0.9 | 49.41 | 50.51 | 39.85 | 58.67 |

### *4.2.2. FG-CNTRC Curved panels under tangential forces*

In this second set of tests, the buckling behavior of simply supported FG-CNTRC curved shells subjected to shear forces has been analyzed. The boundary conditions in the modeling procedure, which ensure a state of pure shear, are given in Table 1. The shear forces have been applied in the form of uniform shell edge loads along the middle surface of plates. Fig. 13 shows the loading types considered in these analyses.

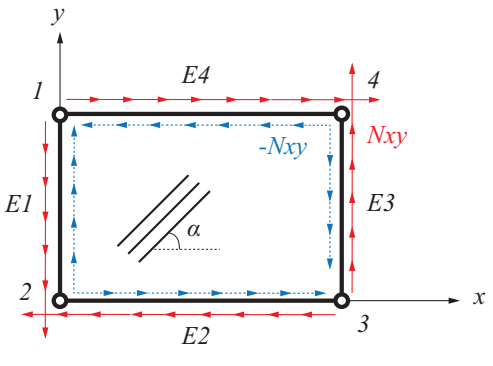


[H]

Figure 13: Positive (+$N_{xy}$) and negative (-$N_{xy}$) shear loading of a FG-CNTRC curved shell.

Table 5: Effect of environment temperature on the buckling load intensity factor ($k_\sigma$=$\sigma_{cr}/\sigma_E$; $\sigma_E$=$\left(\pi^2 E_{(m,T=300K)}/12\left(1-\nu^2_{(m,T=300K)}\right)\right)(t/s)^2$) of FG-CNTRC curved panels under axial compression (SSSS, b=100cm, a=2· b, t=b/50, $V^*_{CNT}$=0.11, $\alpha$=45°).

| T (K) | h/R | $+N_{xy}$ | | | | $-N_{xy}$ | | | |
|---|---|---|---|---|---|---|---|---|---|
| | | UD | FG-V | FG-O | FG-X | UD | FG-V | FG-O | FG-X |
| 300 | 0 | 37.90 | 34.76 | 30.99 | 44.13 | 376.83 | 275.60 | 215.33 | 513.54 |
| | 0.45 | 160.94 | 152.45 | 138.91 | 176.84 | 625.71 | 511.23 | 423.58 | 766.69 |
| | 0.9 | 439.24 | 418.10 | 381.01 | 480.92 | 1341.70 | 1143.93 | 980.55 | 1526.26 |
| 500 | 0 | 24.60 | 22.21 | 19.67 | 28.93 | 317.74 | 237.34 | 188.46 | 417.78 |
| | 0.45 | 99.63 | 94.47 | 86.45 | 107.56 | 455.72 | 383.99 | 325.06 | 526.10 |
| | 0.9 | 269.92 | 257.57 | 236.54 | 292.33 | 865.75 | 791.69 | 710.65 | 897.06 |
| 700 | 0 | 8.00 | 7.03 | 6.15 | 9.42 | 113.54 | 113.97 | 107.83 | 114.13 |
| | 0.45 | 23.21 | 22.65 | 21.60 | 24.28 | 130.79 | 123.61 | 116.47 | 137.50 |
| | 0.9 | 62.72 | 61.09 | 58.23 | 65.80 | 172.77 | 173.17 | 172.41 | 174.17 |

Fig. 14 shows the effect of the fiber angle $\alpha$ on the buckling load factor $k_\sigma$ for square flat and curved shells. The critical loads of the FG-CNTRC panels under negative shear are higher than those of under positive shear for every fiber angle. This is because in the former case the compressive component of the shear is more closely aligned with the fibers. Furthermore, like in the case of compressive loadings, fiber orientation angles aligned with the diagonal of the panels (45°) conduct to higher buckling loads. For further illustration of these results, the first buckling modes of UD-CNTRC panels for different fiber orientation angles and $h/R$ ratios are also depicted in Figs. 15 and 16. Finally, the effect of different temperature environments has been also explored for the case of FG-CNTRC curved panels subjected to shear forces. The results, summarized in Table 5, also show decreases in the buckling load intensity factors as temperature increases

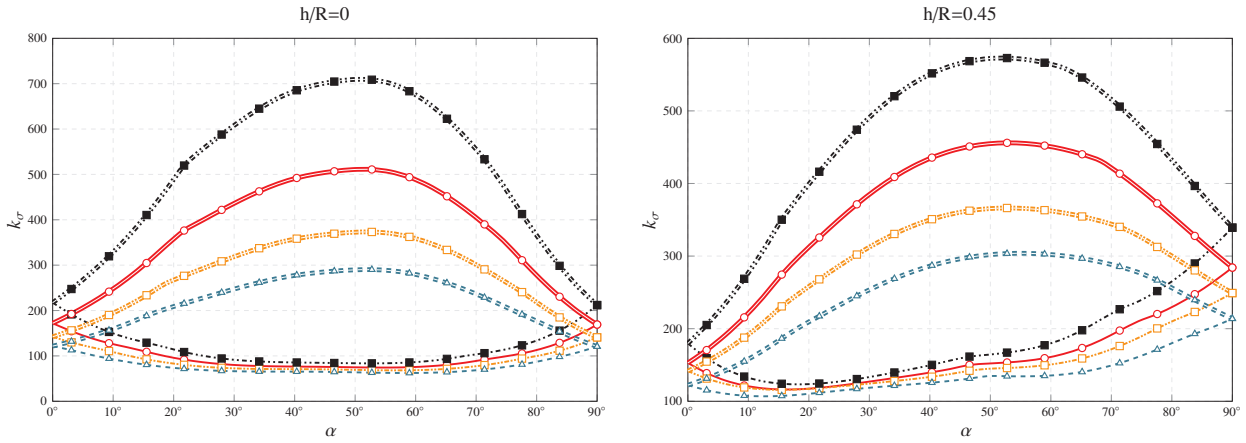


Figure 14: Effect of fiber angle $\alpha$ on the buckling load intensity factor $k_\sigma$ of a FG-CNTRC flat panel subjected to tangential forces ($+N_{xy}$ "-", $-N_{xy}$ "=" ) for different profiles: UD (—○—), FG-V (-·□···), FG-O (- -△- -) and FG-X (- -■-·); (SSSS, b=100cm, a=b, t=b/50, $V^*_{CNT}$=0.11).

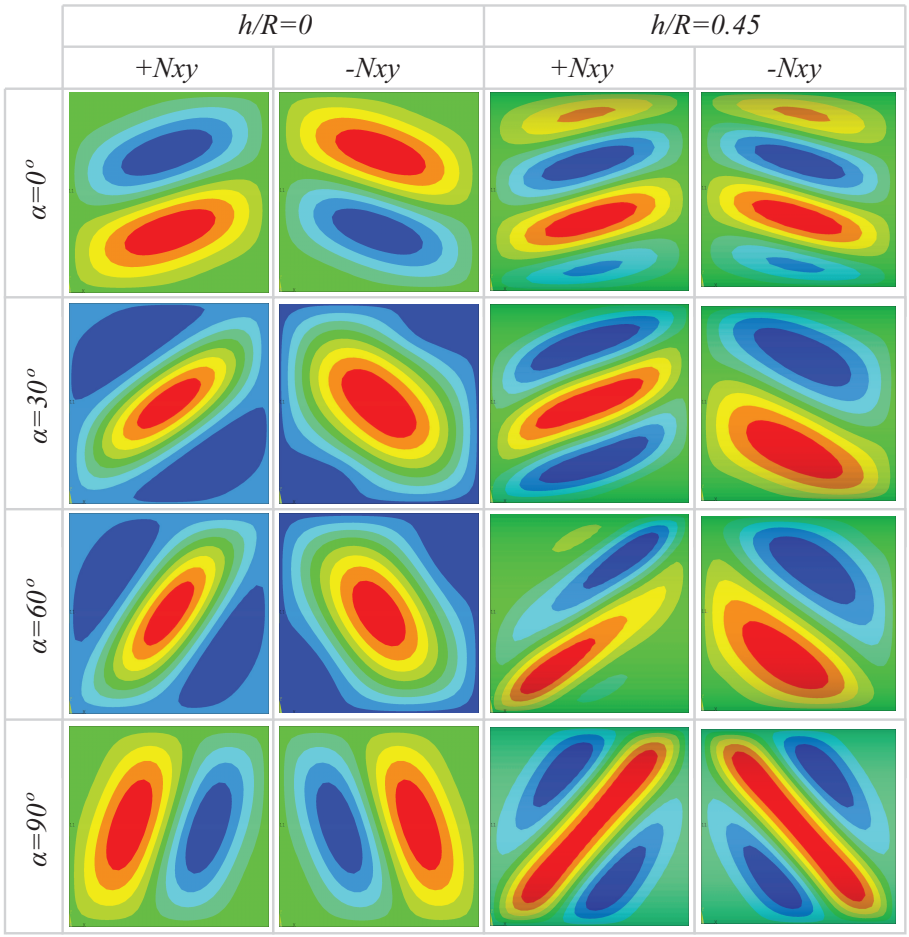


Figure 15: First elastic buckling modes of simply supported UD-CNTRC flat panel (h/R=0) and curved panel (h/R=0.9) under shear forces with different fiber orientation angles $\alpha$ (b=100cm, a=b, t=b/50, $V^*_{CNT}$=0.11).

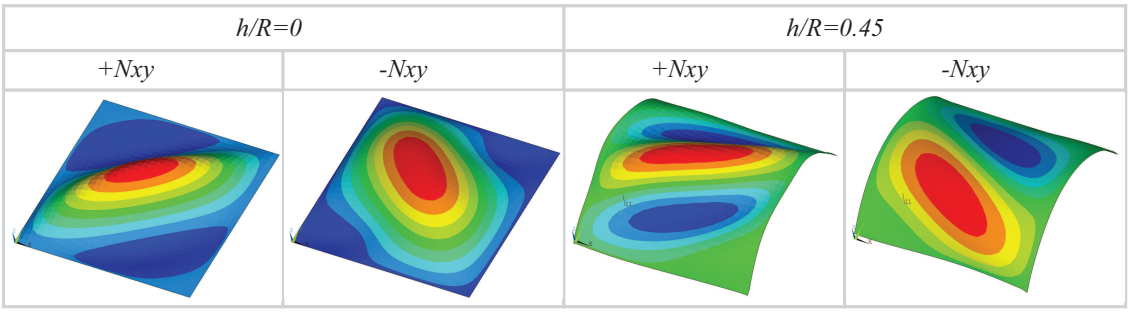


Figure 16: First elastic buckling modes for UD-CNTRC flat panels ($h/R$ = 0) and curved panels ($h/R$ = 0.45) under shear forces with fiber orientation angle ($\alpha$) of 30° under shear forces (SSSS, b=100cm, a=b, t=b/50, $V^*_{CNT}$=0.11).

## 5. Conclusions

In this paper, the critical buckling of FG-CNTRC cylindrical curved panels under compression and shear forces have been investigated by finite elements analyses. The plates are reinforced by SWCNTs and effective material properties of CNTRC plates are estimated either by the Eshelby-Mori-Tanaka approach or the extended rule of mixture. Comparison studies were performed to verify the accuracy and efficiency of the present approach and the results were found to be in good agreement with previously published works. Detailed case studies illustrate the influence of fiber angle, aspect ratio, temperature, SWCNTs grading profile and curvature . The key contributions of this study can be summarized as follows:

- The curvature increases the buckling load values with respect to the flat configuration. This effect is explained by higher circumferential membrane stresses in the radial direction induced by an increasing curvature.
- The buckling load intensity factor $k_\sigma$ of flat panels subjected to compressive loading presents positive curvature with respect to the fiber orientation angle $\alpha$. One clear maximum peak is found for fiber orientations aligned with the diagonal of the panel. On the contrary, the effects of the fiber orientation angle $\alpha$ on the buckling load factor become more complex as the curvature increases. It is shown a change from curves with one single maximum peak to curves with one minimum and two maximum peaks.
- FG-X distribution leads to the largest buckling loads in all the studied cases whilst the FG-O distribution conducts to the minimum values. It is concluded that reinforcements distributed close to the top and bottom induce higher stiffness values.
- In the case of curved panels, it is found some fiber orientation angle ranges in which there is not a big difference among the different CNT distributions. In particular, for curved panels with ratio $h/R$=0.9, in the range of fiber angles between 70° and 85°, all the fiber distributions present very similar results.
- In all cases, the buckling load intensity factors have higher values when the volume fraction of CNT is larger as it raises the stiffness of the panels.
- In the case of curved configurations under compressive loading, slight differences on the buckling loads are found for FG-V and UD distributions with certain values of fiber orientation angle and aspect ratio. This fact even results in the inversion of the relative order of these two distributions.
- The buckling load intensity factors decrease as temperature increases in FG-CNTRC curved panels subjected to compressive and tangential forces as a result of the temperature-dependent material properties.
- The critical loads of the FG-CNTRC panels under the negative shear are higher than those of positive shear for all fiber angles, exhibiting a maximum value for fibers approximately aligned with the diagonal direction ($\alpha = 45°$).


## Acknowledgement

This work was supported by the Ministerio de Economía y Competitividad of Spain and the Consejería de Economía, Innovación, Ciencia y Empleo of Andalucía (Spain) under projects DPI2014-53947-R and P12-TEP-2546. E. G-M was also supported by a FPU contract-fellowship from the Spanish Ministry of Education Ref: FPU13/04892. The financial support is gratefully acknowledged.


## References


[1] A. A. B. Baker, Composite materials for aircraft structures, AIAA, 2004.

[2] J. N. Coleman, U. Khan, W. J. Blau, Y. K. Gunko, Small but strong: A review of the mechanical properties of carbon nanotubepolymer composites, Carbon 44 (2006) 1624–1652.

[3] R. F. Gibson, A review of recent research on mechanics of multifunctional composite materials and structures, Composite Structures 92 (2010) 2793–2810.

[4] F. Ubertini, S. Laflamme, H. Ceylan, A. L. Materazzi, G. Cerni, H. Saleem, A. D'Alessandro, A. Corradini, Novel nanocomposite technologies for dynamic monitoring of structures: a comparison between cement-based embeddable and soft elastomeric surface sensors, Smart Materials and Structures 23 (2014) 045023.

[5] O. Gohardani, M. C. Elola, C. Elizetxea, Potential and prospective implementation of carbon nanotubes on next generation aircraft and space vehicles: A review of current and expected applications in aerospace sciences, Progress in Aerospace Sciences 70 (2014) 42–68.

[6] G. Udupa, S. S. Rao, K. Gangadharan, Functionally graded composite materials: An overview, Procedia Materials Science 5 (2014) 1291–1299.

[7] A. C. Garg, Delamination – a damage mode in composite structures, Engineering Fracture Mechanics 29 (1988) 557–584.

[8] V. V. Bolotin, Delaminations in composite structures: its origin, buckling, growth and stability, Composites Part B: Engineering 27 (1996) 129–145.

[9] N. Kharghani, C. G. Soares, Behavior of composite laminates with embedded delaminations, Composite Structures 150 (2016) 226–239.

[10] S. C. Redshaw, The elastic instability of a thin curved panel subjected to an axial thrust, its axial and circumferential edges being simply supported, HM Stationery Office, 1934.

[11] S. P. Timoshenko, J. M. Gere, Theory of elastic stability, engineering societies monographs, 1961.

[12] E. Z. Stowell, Critical compressive stress for curved sheet supported along all edges and elastically restrained against rotation along the unliaded edges, NACA RB (1943).

[13] H. L. Cox, W. J. Clenshaw, Compression tests on curved plates of thin sheet duralumin, HM Stationery Office, 1941.

[14] H. Crate, L. R. Levin, Data on buckling strength of curved sheet in compression, National Advisory Committee for Aeronautics, 1943.

[15] G. Welter, The effect of radius of curvature and preliminary artificial eccentricities on buckling loads of curved thin aluminum-alloy sheets for monocoque constructions, Journal of the Aeronautical Sciences (2012).

[16] K. Yumura, S. Katsura, K. Ijima, T. Yao, Simulation of buckling collapse behaviour of cylindrically curved plates under axial compression, in: Proceedings of TEAM Conference.

[17] J. S. Park, K. Iijima, T. Yao, Characteristics of buckling and ultimate strength and collapse behaviour of cylindrically curved plates subjected to axial compression, in: Advanced Materials Research, volume 33, Trans Tech Publ, pp. 1195–1200.

[18] J.-S. Park, M. Fujikubo, K. Iijima, T. Yao, et al., Prediction of the secondary buckling strength and ultimate strength of cylindrically curved plate under axial compression, in: The Nineteenth International Offshore and Polar Engineering Conference, International Society of Offshore and Polar Engineers.

[19] K. Le Tran, L. Davaine, C. Douthe, K. Sab, Stability of curved panels under uniform axial compression, Journal of constructional steel research 69 (2012) 30–38.

[20] D. Leggett, The elastic stability of a long and slightly bent rectangular plate under uniform shear, Proceedings of the Royal Society of London. Series A, Mathematical and Physical Sciences (1937) 62–83.

[21] A. Kromm, The limit of stability of a curved plate strip under shear and axial stresses (1939).

[22] S. Batdorf, M. Stein, M. Schildcrout, Critical shear stress of curved rectangular panels, Technical Report, 1947.

[23] H. Wang, J. G. Croll, Optimisation of shell buckling using lower bound capacities, Thin-Walled Structures 46 (2008) 1011–1020.

[24] M. Amani, B. Edlund, M. M. Alinia, Buckling and postbuckling behavior of unstiffened slender curved plates under uniform shear, Thin-Walled Structures 49 (2011) 1017–1031.

[25] H. Shen, Nonlinear bending of functionally graded carbon nanotube-reinforced composite plates in thermal environments, Composite Structures 91 (2009) 9–19.

[26] H. S. Shen, C. L. Zhang, Thermal buckling and postbuckling behavior of functionally graded carbon nanotube-reinforced composite plates, Materials & Design 31 (2010) 3403–3411.

[27] A. G. Arani, S. Maghamikia, M. Mohammadimehr, A. Arefmanesh, Buckling analysis of laminated composite rectangular plates reinforced by SWCNTs using analytical and finite element methods, Journal of Mechanical Science and Technology 25 (2011) 809–820.

[28] S. J. Mehrabadi, B. S. Aragh, V. Khoshkhahesh, A. Taherpour, Mechanical buckling of nanocomposite rectangular plate reinforced by aligned and straight single-walled carbon nanotubes, Composites Part B: Engineering 43 (2012) 2031–2040.

[29] Z. X. Lei, K. M. Liew, J. L. Yu, Buckling analysis of functionally graded carbon nanotube-reinforced composite plates using the element-free kp-Ritz method, Composite Structures 98 (2013) 160–168.

[30] P. Zhu, L. W. Zhang, K. M. Liew, Geometrically nonlinear thermomechanical analysis of moderately thick functionally graded plates using a local petrov–galerkin approach with moving kriging interpolation, Composite Structures 107 (2014) 298–314.

[31] L. W. Zhang, P. Zhu, K. M. Liew, Thermal buckling of functionally graded plates using a local kriging meshless method, Composite Structures 108 (2014) 472–492.

[32] Z. X. Lei, L. W. Zhang, K. M. Liew, Buckling of FG-CNT reinforced composite thick skew plates resting on pasternak foundations based on an element-free approach, Applied Mathematics and Computation 266 (2015) 773–791.

[33] L. W. Zhang, Z. X. Lei, K. M. Liew, An element-free IMLS-Ritz framework for buckling analysis of FG-CNT reinforced composite thick plates resting on winkler foundations, Engineering Analysis with Boundary Elements 58 (2015) 7–17.

[34] L. W. Zhang, K. M. Liew, Postbuckling analysis of axially compressed CNT reinforced functionally graded composite plates resting on pasternak foundations using an element-free approach, Composite Structures 138 (2016) 40–51.

[35] L. W. Zhang, Z. X. Lei, K. M. Liew, Buckling analysis of FG-CNT reinforced composite thick skew plates using an element-free approach, Composites Part B: Engineering 75 (2015) 36–46.

[36] L. W. Zhang, K. M. Liew, J. N. Reddy, Postbuckling of carbon nanotube reinforced functionally graded plates with edges elastically restrained against translation and rotation under axial compression, Computer Methods in Applied Mechanics and Engineering 298 (2016) 1–28.

[37] L. W. Zhang, K. M. Liew, J. N. Reddy, Postbuckling behavior of bi-axially compressed arbitrarily straight-sided quadrilateral functionally graded material plates, Computer Methods in Applied Mechanics and Engineering 300 (2016) 593–610.

[38] Z. X. Lei, L. W. Zhang, K. M. Liew, Free vibration analysis of laminated FG-CNT reinforced composite rectangular plates using the kp-ritz method, Composite Structures 127 (2015) 245–259.

[39] L. W. Zhang, Y. Zhang, G. L. Zou, K. M. Liew, Free vibration analysis of triangular CNT-reinforced composite plates subjected to in-plane stresses using FSDT element-free method, Composite Structures 149 (2016) 247–260.

[40] L. W. Zhang, K. M. Liew, Geometrically nonlinear large deformation analysis of functionally graded carbon nanotube reinforced composite straight-sided quadrilateral plates, Computer Methods in Applied Mechanics and Engineering 295 (2015) 219–239.

[41] L. W. Zhang, W. C. Cui, K. M. Liew, Vibration analysis of functionally graded carbon nanotube reinforced composite thick plates with elastically restrained edges, International Journal of Mechanical Sciences 103 (2015) 9–21.

[42] L. W. Zhang, Z. G. Song, K. M. Liew, Nonlinear bending analysis of FG-CNT reinforced composite thick plates resting on Pasternak foundations using the element-free IMLS-Ritz method, Composite Structures 128 (2015) 165–175.

[43] L. W. Zhang, Z. G. Song, K. M. Liew, State-space levy method for vibration analysis of FG-CNT composite plates subjected to in-plane loads based on higher-order shear deformation theory, Composite Structures 134 (2015) 989–1003.

[44] Z. Lei, L. Zhang, K. Liew, J. Yu, Dynamic stability analysis of carbon nanotube-reinforced functionally graded cylindrical panels using the element-free kp-Ritz method, Composite Structures 113 (2014) 328–338.

[45] H. S. Shen, Y. Xiang, Postbuckling of axially compressed nanotube-reinforced composite cylindrical panels resting on elastic foundations in thermal environments, Composites Part B: Engineering 67 (2014) 50–61.

[46] K. Liew, Z. Lei, L. Zhang, Mechanical analysis of functionally graded carbon nanotube reinforced composites: a review, Composite Structures 120 (2015) 90–97.

[47] D. Shi, X. Feng, Y. Y. Huang, K. Hwang, H. Gao, The effect of nanotube waviness and agglomeration on the elastic property of carbon nanotube-reinforced composites, Journal of Engineering Materials and Technology 126 (2004) 250–257.

[48] A. M. Esawi, M. M. Farag, Carbon nanotube reinforced composites: potential and current challenges, Materials & Design 28 (2007) 2394–2401.

[49] J. Fidelus, E. Wiesel, F. Gojny, K. Schulte, H. Wagner, Thermo-mechanical properties of randomly oriented carbon/epoxy nanocomposites, Composites Part A: Applied Science and Manufacturing 36 (2005) 1555–1561.

[50] B. Sobhani Aragh, A. Nasrollah Barati, H. Hedayati, Eshelby-Mori-Tanaka approach for vibrational behavior of continuously graded carbon nanotube-reinforced cylindrical panels, Composites Part B: Engineering 43 (2012) 1943–1954.

[51] T. Mori, K. Tanaka, Average stress in matrix and average elastic energy of materials with misfitting inclusions, Acta metallurgica 21 (1973) 571–574.

[52] J. D. Eshelby, The determination of the elastic field of an ellipsoidal inclusion, and related problems, Proceedings of the Royal Society of London. Series A. Mathematical and Physical Sciences 241 (1957) 376–396.

[53] J. Eshelby, The elastic field outside an ellipsoidal inclusion, Proceedings of the Royal Society of London. Series A, Mathematical and Physical Sciences (1959) 561–569.

[54] Y. Benveniste, A new approach to the application of Mori-Tanaka's theory in composite materials, Mechanics of materials 6 (1987) 147–157.

[55] T. Mura, Micromechanics of defects in solids, volume 3, Springer, 1987.

[56] F. Tornabene, N. Fantuzzi, M. Bacciocchi, E. Viola, Effect of agglomeration on the natural frequencies of functionally graded carbon nanotube-reinforced laminated composite doubly-curved shells, Composites Part B: Engineering 89 (2016) 187–218.

[57] Structural analysis guide, Release 15.0, ANSYS Inc, Cannonsburg, PA (2014).

[58] E. Efraim, M. Eisenberger, Exact vibration analysis of variable thickness thick annular isotropic and FGM plates, Journal of Sound and Vibration 299 (2007) 720–738.

[59] V. Popov, V. Van Doren, M. Balkanski, Elastic properties of crystals of single-walled carbon nanotubes, Solid State Communications 114 (2000) 395–399.

[60] Y. Han, J. Elliott, Molecular dynamics simulations of the elastic properties of polymer/carbon nanotube composites, Computational Materials Science 39 (2007) 315–323.

[61] I. Hwang, J. S. Lee, Buckling of orthotropic plates under various inplane loads, KSCE Journal of Civil Engineering 10 (2006) 349–356.

[62] M. M. Domb, B. R. Leigh, Refined design curves for compressive buckling of curved panels using nonlinear finite element analysis, in: AIAA/ASME/ASCE/AHS/ASC Structures, Structural Dynamics, and Materials Conference and Exhibit, 42 nd, Seattle, WA.

[63] F. Tornabene, N. Fantuzzi, M. Bacciocchi, Linear static response of nanocomposite plates and shells reinforced by agglomerated carbon nanotubes, Composites Part B: Engineering (2016). 10.1016/j.compositesb.2016.07.011.

[64] S. Kamarian, M. Salim, R. Dimitri, F. Tornabene, Free vibration analysis of conical shells reinforced with agglomerated carbon nanotubes, International Journal of Mechanical Sciences 108 (2016) 157–165.

[65] E. García-Macías, R. Castro-Triguero, E. I. S. Flores, M. I. Friswell, R. Gallego, Static and free vibration analysis of functionally graded carbon nanotube reinforced skew plates, Composite Structures (2016).